PAPER

Ferrocenyl-L-amino acid copper(II) complexes showing remarkable photo-induced anticancer activity in visible light†

Tridib K. Goswami,[a] Sudarshan Gadadhar,[b] Babu Balaji,[a] Bappaditya Gole,[a] Anjali A. Karande*[b] and Akhil R. Chakravarty*[a]

Ferrocene-conjugated copper(II) complexes [Cu(Fc-aa)(aip)](ClO$_4$) (**1–3**) and [Cu(Fc-aa)(pyip)](ClO$_4$) (**4–6**) of L-amino acid reduced Schiff bases (Fc-aa), 2-(9-anthryl)-1*H*-imidazo[4,5-*f*][1,10]phenanthroline (aip) and 2-(1-pyrenyl)-1*H*-imidazo[4,5-*f*][1,10]phenanthroline (pyip), where Fc-aa is ferrocenylmethyl-L-tyrosine (Fc-Tyr in **1**, **4**), ferrocenylmethyl-L-tryptophan (Fc-Trp in **2**, **5**) and ferrocenylmethyl-L-methionine (Fc-Met in **3**, **6**), were prepared and characterized, and their photocytotoxicity was studied (Fc = ferrocenyl moiety). Phenyl analogues, *viz.* [Cu(Ph-Met)(aip)](ClO$_4$) (**7**) and [Cu(Ph-Met)(pyip)](ClO$_4$) (**8**), were prepared and used as control compounds. The bis-imidazophenanthroline copper(II) complexes, *viz.* [Cu(aip)$_2$(NO$_3$)](NO$_3$) (**9**) and [Cu(pyip)$_2$(NO$_3$)](NO$_3$) (**10**), were also prepared and used as controls. Complexes **1–6** having a redox inactive cooper(II) center showed the Fc$^+$–Fc redox couple at ~0.5 V *vs.* SCE in DMF–0.1 mol [Bu$^n_4$N](ClO$_4$). The copper(II)-based d–d band was observed near 600 nm in DMF–Tris-HCl buffer (1 : 1 v/v). The ferrocenyl complexes showed low dark toxicity, but remarkably high photocytotoxicity in human cervical HeLa and human breast adenocarcinoma MCF-7 cancer cells giving an excellent photo-dynamic effect while their phenyl analogues were inactive. The photo-exposure caused significant morphological changes in the cancer cells when compared to the non-irradiated ones. The photophysical processes were rationalized from the theoretical studies. Fluorescence microscopic images showed **3** and **6** localizing predominantly in the endoplasmic reticulum (ER) of the cancer cells, thus minimizing any undesirable effects involving nuclear DNA.

Introduction

Photodynamic therapy (PDT) using metal complexes has received considerable current interest as a potential alternative to the organic dye-based PDT for the treatment of cancer.[1–20] Porphyrin bases like FDA approved drug Photofrin® show undesirable prolonged skin photosensitivity and hepatotoxicity.[21] Additionally the efficacy of such organic dyes is dependent on their ability to generate singlet oxygen species *via* the type-II energy transfer process. In contrast, metal-based PDT agents could follow the alternate type-I and/or photo-redox process to generate other cytotoxic reactive oxygen species

[a]*Department of Inorganic and Physical Chemistry, Indian Institute of Science, Bangalore 560012, India. E-mail: arc@ipc.iisc.ernet.in; Tel: +91-80-22932533*
[b]*Department of Biochemistry, Indian Institute of Science, Bangalore 560012, India. E-mail: anjali@biochem.iisc.ernet.in; Tel: +91-80-22932306*
†Electronic supplementary information (ESI) available: Synthesis, characterization, DNA binding and cleavage, cellular and DFT data (Schemes S1–S3, Fig. S1–S30, Tables S1–S4). See DOI: 10.1039/c4dt01348d

(ROS).[22] A number of Pt(IV), Rh(II) and Ru(II) complexes are reported to show a significant photo-induced cytotoxic effect in a variety of cancer cells following different reaction pathways.[6–12,15] Sadler and co-workers reported photocytotoxic Pt(IV) complexes that on photo-activation generate cytotoxic Pt(II) species showing antitumor activity even for cisplatin resistant cancer cells.[15] NO and CO releasing metal complexes are shown to be highly effective in damaging cancer cells on photo-activation.[3] We recently reported oxovanadium(IV) and iron(III) complexes as potential metal-based photocytotoxic agents showing visible light-induced cellular damage in various cancer cells.[16–20] Porphyrin bases including Photofrin® are known to target the mitochondria to damage the cancer cells, whereas cisplatin and its analogues are known to induce cross-linking of nuclear DNA resulting in apoptotic cell death.[1,11,15,23,24] Another possibility of cell death is by compounds targeting the endoplasmic reticulum (ER) which is a vital cellular component involved in key cellular functions like correct folding of proteins and their transport to other organelles. The ER stress response (ERSR) caused by reactive

oxygen species (ROS) damages the cancer cells *via* the intrinsic pathway of apoptosis involving the mitochondria without affecting the nuclear DNA.[25–29]

The present work stems from our continued interest in designing ferrocenyl complexes as potent organometallic photocytotoxic agents. Although organometallic complexes were earlier investigated for their anticancer applications, their utility in PDT is yet to be fully realized.[30–39] Introducing classical organometallic moieties into known drugs or lead compounds could provide a novel strategy towards designing bioorganometallic anticancer agents. The ferrocene-appended breast cancer drug tamoxifen is known to exhibit the desirable activity in both hormone dependent and independent breast cancers whereas the parent drug fails in the hormone independent case.[39] The organometallic PDT agents are of recent origin.[40–47] It has been observed that ferrocene-appended copper(II) and oxovanadium(IV) complexes provide a significant improvement in the photocytotoxic activity when compared to the controls that lack the ferrocenyl moiety. This has prompted us to explore this chemistry further using copper(II) complexes containing organometallic pendants.

Dark toxicity remained a major problem associated with the metal complexes having redox active metal centers. Among them, copper(II) complexes are known to show undesirable high dark toxicity in cells.[48,49] Cellular thiols can easily reduce copper(II) to copper(I) and hence there is continuous generation of radicals that damage the cells. This poses a major obstacle for their cellular applications in PDT. However, it is possible to tune the redox activity of a metal center in a complex by suitable ligand design. To this end, we have tried to reduce the redox activity of the ferrocene-appended L-amino acid reduced Schiff base copper(II) complexes by introducing electron rich anthracenyl and pyrenyl imidazophenanthroline ligands. These electron rich ligands are likely to stabilize the copper(II) center to a great extent and hence its reduction to the copper(I) species by cellular thiols gets significantly reduced. Besides, our design for a ternary structure has resulted in sterically constrained copper(II) complexes for which conversion to the copper(I) species becomes unfavorable and this has reduced the dark toxicity of the complexes while retaining their phototoxicity in the cancer cells. Being fluorescent, both anthracenyl and pyrenyl imidazophenanthroline ligands enabled us to study localization of the complexes in the cancer cells.

Herein, we describe the synthesis, characterization, DNA binding affinity, photo-induced DNA cleavage activity and photo-enhanced cytotoxicity of six ferrocene-appended reduced Schiff base (Fc-aaH) copper(II) complexes of L-amino acids and (anthracenyl)/(pyrenyl)imidazophenanthroline bases, *viz*. [Cu(Fc-aa)(aip)](ClO₄) (**1–3**) and [Cu(Fc-aa)(pyip)]- (ClO₄) (**4–6**), where Fc-aa is ferrocenylmethyl-L-tyrosine (Fc-Tyr in **1**, **4**), ferrocenylmethyl-L-tryptophan (Fc-Trp in **2**, **5**), and ferrocenylmethyl-L-methionine (Fc-Met in **3**, **6**), aip is 2-(9-anthryl)-1*H*-imidazo[4,5-*f*][1,10]phenanthroline (in **1–3**) and pyip is 2-(1-pyrenyl)-1*H*-imidazo[4,5-*f*][1,10]phenanthroline (in **4–6**) (Fig. 1). Complexes [Cu(Ph-Met)(aip)](ClO₄) (**7**), [Cu(Ph-Met)(pyip)](ClO₄) (**8**), [Cu(aip)₂(NO₃)](NO₃) (**9**) and [Cu(pyip)₂-

Fig. 1 Schematic drawings of the complexes [Cu(Fc-aa)(aip/pyip)]- (ClO₄) and [Cu(Ph-Met)(aip/pyip)](ClO₄) (aip in **1–3**, **7**; pyip in **4–6**, **8**), where Fc-aa is Fc-Tyr (in **1** and **4**), Fc-Trp (in **2** and **5**) and Fc-Met (in **3** and **6**).

(NO₃)](NO₃) (**10**) were synthesized and used as control species for cellular experiments. Significant results include high DNA binding affinity of the complexes, low chemical nuclease activity and DNA photocleavage activity in visible light at low complex concentrations, and remarkable visible light-induced cytotoxicity of the ferrocenyl complexes **1–6** in HeLa and MCF-7 cancer cells through induction of apoptosis while remaining less toxic in the dark. The control complexes **7–10** did not show any photocytotoxicity under similar assay conditions. Our observation of the PDT effect of the ferrocenyl-copper(II) complexes with unprecedented low dark toxicity is novel and this is achieved from the rigid square-planar/square pyramidal geometry of the copper(II) centers out of serendipity with one or both axial sites blocked by the pendant groups. In addition, fluorescence microscopy images of the complexes having anthracenyl and pyrenyl imidazophenanthroline ligands reveal significant cytosolic localization of **3** and **6** in the cancer cells. The cytosolic localization which models the cellular uptake of the successful PDT agents is preferred by the oncologists to avoid any possible mutation of DNA in the case of nuclear localization.[24] The fortuitous observation of selective localization of the complexes in the endoplasmic reticulum (ER) and cellular damage by ROS is of novelty considering this mode of apoptosis being preferred in PDT over the nuclear DNA damage.[50–52]
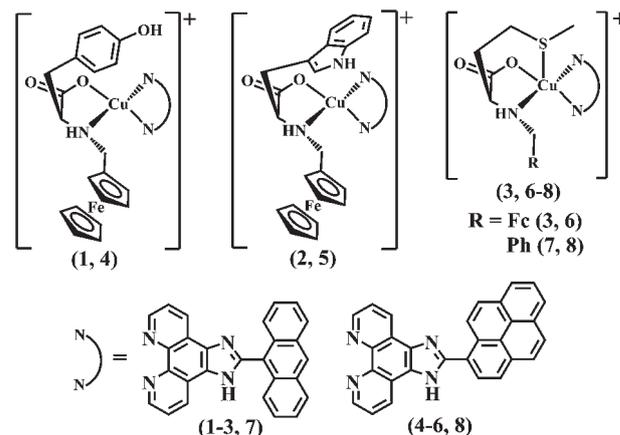
Results and discussion

Synthesis and general properties

Ternary copper(II) complexes having ferrocene-conjugated L-amino acid reduced Schiff bases and the anthracenyl imidazophenanthroline (aip) or pyrenyl imidazophenanthroline (pyip) ligand, namely, [Cu(Fc-aa)(aip)](ClO₄) (**1–3**) and [Cu(Fc-aa)(pyip)](ClO₄) (**4–6**), where Fc-aa is Fc-Tyr (**1**, **4**), Fc-Trp (**2**, **5**) or Fc-Met (**3**, **6**), were synthesized in high yield from the reaction of the ferrocenylmethyl-L-amino acid ligand with

copper(II) acetate monohydrate and aip or pyip in methanol (Fig. 1, Fig. S1–S4, ESI†). Complexes **7** and **8** having the Ph-Met ligand and binary copper(II) complexes of aip/pyip were prepared as controls. The complexes were characterized from the spectral and analytical data. Selected physicochemical data are given in Table 1. The stability of the complexes in the solution phase was studied from their ESI-MS spectra displaying essentially the molecular ion peak as $[M - (ClO_4)]^+$ in methanol (Fig. S5–S10, ESI†). The IR spectra of the complexes showed characteristic stretching bands at ~1640 and ~1360 cm^{-1} due to asymmetric and symmetric COO stretch respectively along with a ClO_4^- stretching band at ~1085 cm^{-1}. The complexes are 1:1 electrolytic with the molar conductance value of ~80 S m^2 mol^{-1} in DMF at 25 °C. The magnetic moment value of ~1.8μ_B at 25 °C suggests the presence of a one-electron paramagnetic 3d^9-Cu(II) center in the complexes. The electronic spectra of the complexes in DMF–Tris-HCl buffer (1:1 v/v) displayed a broad and weak copper-centered d–d band in the range of 600–620 nm. The spectra of **1–3** having the anthracenyl imidazophenanthroline (aip) ligand are characterized by low intensity π→π* bands at ~370 nm along with a shoulder at ~385 nm, whereas complexes **4–6** having the pyrenyl imidazophenanthroline ligand displayed the π→π* transition at ~372 nm along with a shoulder at ~400 nm. The high-energy π→π* transitions corresponding to the phenanthroline moiety of the ligands appeared at ~253 nm for **1–3** and ~245 nm and ~285 nm for **4–6** (Fig. 2, Fig. S11, ESI†).[53] The anthracenyl and pyrenyl ligand-centered bands with high extinction coefficient values mask the relatively weak ferrocene-based band that generally appears near 450 nm. Complexes **1–3** having the anthracenyl imidazophenanthroline ligand exhibited an emission spectral band at 475 nm on excitation at 370 nm in DMF–Tris-HCl buffer (1:1 v/v) at 25 °C with respective quantum yield (φ) values of 0.07, 0.08 and 0.08 in DMF. The pyrenyl imidazophenanthroline complexes **4–6** showed an emission band at 450 nm on excitation at 370 nm with a relatively higher quantum yield (φ) value of 0.10, 0.10 and 0.12 in DMF under similar experi-
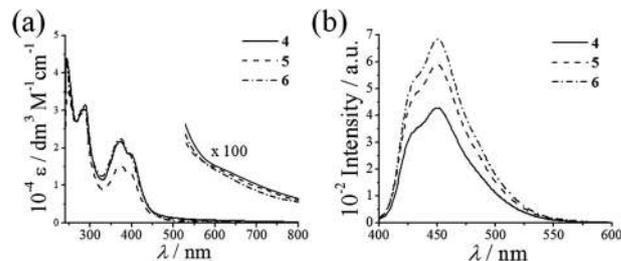

Fig. 2 (a) Electronic absorption and (b) emission (λ_{ex} = 370 nm) spectra of [Cu(Fc-aa)(pyip)](ClO$_4$) (Fc-aa = Fc-Tyr, **4**; Fc-Trp, **5**; Fc-Met, **6**) in DMF–Tris-HCl buffer (1:1 v/v).

mental conditions (Fig. 2). The emissive property of the complexes was utilized for cellular localization study by fluorescence microscopy. The complexes showed a quasi-reversible response for the Fc$^+$–Fc couple (Fc, ferrocenyl moiety) at ~0.5 V vs. SCE in DMF–0.1 mol TBAP while being redox inactive at the copper(II) center (Fig. S12, ESI†). A significant positive shift of ~100 mV of the Fe(III)–Fe(II) potential is observed in the ferrocenyl complexes compared to that of ferrocene (0.43 V).

Energy optimized structures

We have performed optimization of the structures of the complexes **1–6** from density functional theory (DFT) calculations (Fig. S13, Tables S1 and S2, ESI†).[54,55] The optimized structures showed similar structural characteristics to that observed in the crystal structures of [Cu(Fc-Phe)(phen)](ClO$_4$) (Fc-phe = ferrocenylmethyl-L-phenylalanine), [Cu(Fc-Trp)(bpy)](ClO$_4$) (bpy = 2,2′-bipyridine) and [Cu(Fc-Met)(phen)](PF$_6$).[47] The copper(II) center in the Fc-tyr and Fc-trp complexes has a square-planar geometry with a CuN$_3$O coordination environment having two axial sites sterically blocked by the pendant group of the amino acid and the ferrocenyl moiety. The Cu(II) centre in complexes **3** and **6** has the Fc-met ligand in a square-pyramidal geometry showing a CuN$_3$OS coordination environment with the sulfur atom of the thiomethyl pendant moiety of L-methionine occupying the fifth coordination site. There is a large deviation from planarity in aip and pyip with the plane of the anthracenyl or pyrenyl group making a respective di-

Table 1 Selected physicochemical data for the complexes [Cu(Fc-aa)(aip)](ClO$_4$) (**1–3**) and [Cu(Fc-aa)(pyip)](ClO$_4$) (**4–6**)

Complex	IR/cm^{-1} [ν(ClO$_4^-$)]	λ_{max}/nm (ε/dm^3 mol^{-1} cm^{-1})^a	E_f/V (ΔE_p/mV)^b (Fc$^+$–Fc)	$\Lambda_M{}^c$/ S m^2 mol^{-1}	$\mu_{eff}{}^d$/ μ_B
1	1085	605 (145)	0.51 (150)	85	1.82
2	1085	600 (150)	0.50 (100)	83	1.80
3	1087	600 (135)	0.52 (130)	79	1.79
4	1095	615 (140)	0.51 (140)	78	1.81
5	1095	615 (130)	0.50 (120)	82	1.78
6	1090	620 (140)	0.50 (120)	79	1.77

^{a} In DMF–Tris-HCl buffer (1:1 v/v). The d–d band at ~600 nm is copper(II)-centered. The ferrocene-centered band at ~450 nm is masked by strong ligand-centered bands. ^{b} The Fc$^+$–Fc redox couple in DMF–0.1 M TBAP. $E_f = 0.5(E_{pa} + E_{pc})$, $\Delta E_p = (E_{pa} - E_{pc})$, where E_{pa} and E_{pc} are the anodic and cathodic peak potentials, respectively. The potentials vs. SCE. Scan rate = 50 mV s^{-1}. ^{c} The molar conductivity in DMF. ^{d} The magnetic moment at 298 K using a DMSO-d_6 solution of the complexes.
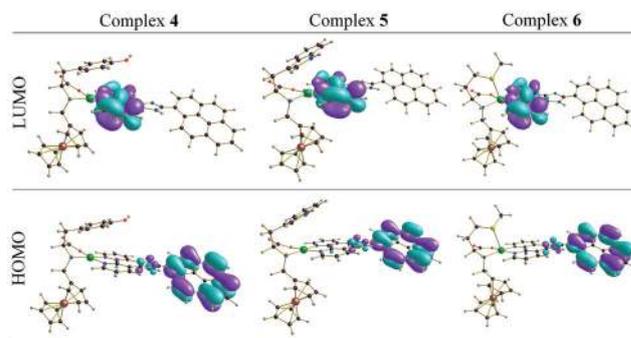

Fig. 3 HOMO and LUMO of the complexes **4–6** with a contour value of 0.03 a.u.

hedral angle of ~50° and ~40° with the plane of the imidazo-phenanthroline ring due to steric constraints.

The HOMO and LUMO of the complexes are shown in Fig. 3 (Fig. S14, ESI†). The HOMO–LUMO energy gap in **1–6** is ~2.2 eV (Table S3, ESI†). It is evident that the HOMOs are largely localized on the anthracene or pyrene moiety of the complexes. The LUMOs are the vacant orbital largely localized on the phenanthroline moiety and this could result in a charge transfer on photo-excitation from the anthracene or pyrene moiety to the phenanthroline which is coordinated to the Cu(II) centre.

DNA binding and cleavage properties

DNA being a potential target for the mitochondria mediated apoptosis, the affinity of the complexes to bind calf-thymus (ct) DNA was studied using spectral, DNA melting and visco-metric methods. Selected ct-DNA binding data are given in Table 2. The results suggest that **1–6** are excellent binders to ct-DNA probably through intercalation to the DNA base pairs. The intrinsic DNA binding constant (K_b) of the complexes determined by the UV-visible absorption titration method gives the K_b values within $(6.8 \pm 0.5) \times 10^5$ to $(7.9 \pm 0.6) \times 10^6$ mol^{-1} with the order of DNA binding strength as: **6 ~ 5 ~ 4 > 3 ~ 2 ~ 1** (Table 2, Fig. S15, ESI†). The extended aromatic π-system of the anthracenyl and pyrenyl imidazophenanthroline ligands seems to facilitate intercalation of the ligand to the DNA base pairs through the groove resulting in higher binding strengths.[56] To further explore the DNA binding propensity of the complexes, the DNA melting experiments were carried out. Complexes **4–6** having the pyrenyl imidazophen-anthroline ligand stabilized ct-DNA to a significant extent giving a ΔT_m value in the range of 2.6–5.7 °C. The extent of increase in the ΔT_m parallels the intercalative DNA binding strength of the ligand. The classical DNA intercalator ethidium bromide (EB) gave a ΔT_m value of ~15 °C under similar experimental conditions due to its high intercalative binding affinity to DNA (Table 2, Fig. S16, ESI†).[57] Viscometric titration experiments were performed to further elucidate the mode and affinity of the complexes for DNA binding by monitoring the change in the relative specific viscosity of the ct-DNA in the presence of the complexes. The plots of relative viscosity $(\eta/\eta_0)^{1/3}$, where η and η_0 are the respective specific viscosity of DNA in the presence and absence of the complex, vs. [complex]/[DNA] ratio for **1–6** and their comparisons with EB and the groove binder Hoechst dye show a significant change in the relative specific viscosity of ct-DNA on treating with the

complexes thus indicating an intercalative mode of DNA binding of the complexes (Fig. S16, ESI†).[58]

The ability of the complexes **1–6** (5 μmol) to cleave super-coiled (SC) DNA was studied in the presence of glutathione (GSH, 1.0 mmol) as an external reducing agent and hydrogen peroxide (H$_2$O$_2$, 200 μmol) as an oxidizing agent using pUC19 DNA (0.2 μg, 30 μM b.p. (base pairs)) in 50 mmol Tris-HCl–50 mmol NaCl buffer (pH 7.2) (Fig. S17, ESI†). Electrochemical data showed that the complexes are redox inactive at the copper(II) center. This is evidenced from no apparent chemical nuclease activity of the complexes in the presence of GSH. Copper(II) complexes are generally known to show high chemi-cal nuclease activity thus restricting their application in PDT in a cellular medium having reducing thiols.[59] For example, a 5 μmol solution of [Cu(phen)$_2$(NO$_3$)](NO$_3$) essentially comple-tely converted SC DNA to its NC form for an incubation period of 2 h under similar experimental conditions. In addition, the present complexes did not show any significant nuclease activity in the presence of H$_2$O$_2$. Thus by choosing suitable ligand systems the undesirable chemical nuclease activity of the copper(II) complexes could be minimized to a significant extent thus making the complexes suitable for potential cellu-lar applications in PDT.

The DNA photocleavage experiments were performed using complexes **1–6** and SC pUC19 DNA (30 μmol b.p., 0.2 μg) in Tris-HCl–NaCl buffer (50 mmol, pH 7.2). Monochromatic blue, green and red light of 454 nm (50 mW), 568 nm (50 mW) and 647 nm (50 mW) wavelengths was used from a tunable con-tinuous-wave (CW) Ar–Kr mixed-gas ion laser for DNA photo-cleavage studies (Fig. S18, ESI†). Control experiments showed no apparent photocleavage of DNA alone in visible light. None of the complexes gave any significant nicking of SC-DNA to its NC-form in the dark, thus eliminating the possibility of any hydrolytic damage of DNA or generation of any reactive species that can damage DNA in the dark. A 10 μmol solution of the anthracenyl imidazophenanthroline complexes **1–3** showed significant DNA photocleavage activity in blue light of 454 nm for an irradiation time of 2 h giving ~80% NC form. The pyrenyl imidazophenanthroline complexes **4–6** showed better photonuclease activity in blue light cleaving ~90% of SC DNA. The higher activity of **4–6** can be rationalized on the basis of their higher DNA binding strengths and/or higher photo-activity at this wavelength in the presence of a larger planar π-system of pyrene. The photonuclease activity of the com-plexes at 454 nm blue light follows the order: **6** (Fc-Met-Cu-pyip) > **5** (Fc-Trp-Cu-pyip) ~ **4** (Fc-Tyr-Cu-pyip) > **3** (Ph-Met-Cu-

Table 2 DNA binding data of the complexes [Cu(Fc-aa)(aip)](ClO$_4$) (**1–3**) and [Cu(Fc-aa)(pyip)](ClO$_4$) (**4–6**)

	1	2	3	4	5	6
$K_b{}^a$ /mol^{-1}	$(6.8 \pm 0.5) \times 10^5$	$(7.5 \pm 0.4) \times 10^5$	$(7.7 \pm 0.7) \times 10^5$	$(6.3 \pm 0.4) \times 10^6$	$(7.7 \pm 0.6) \times 10^6$	$(7.9 \pm 0.6) \times 10^6$
$[s]^b$	[0.16]	[0.16]	[0.19]	[0.26]	[0.30]	[0.31]
$\Delta T_m{}^c$/°C	2.6	3.1	2.8	5.2	5.5	5.7

[a] The intrinsic equilibrium DNA binding constant from the UV-visible experiment. [b] The MvH equation fitting parameter (ref. 73). [c] The change in the calf thymus DNA melting temperature.

Table 3 Selected DNA (SC pUC19, 0.5 μg) cleavage data for [Cu(Fc-aa)-(aip)](ClO₄) (**1–3**) and [Cu(Fc-aa)(aip)](ClO₄) (**4–6**) in visible light

Reaction conditions[a]	%NC form (λ = 454 nm)	%NC form (λ = 568 nm)	%NC form (λ = 647 nm)
DNA control	2	3	2
DNA + **1**	78	67	62
DNA + **2**	85	70	69
DNA + **3**	82	76	68
DNA + **4**	88	79	77
DNA + **5**	95	85	86
DNA + **6**	97	88	89

[a] In Tris-buffer medium (pH = 7.2). λ, laser wavelength. Photo-exposure time (t) = 2 h. The concentration of the complexes **1–6** was 10 μmol for the 454 nm and 15 μmol for the 568 and 647 nm experiments.

Fig. 4 Cell viability plots showing the cytotoxic effect of (a) complex **3** in HeLa cells, (b) complex **3** in MCF-7 cells, (c) complex **6** in HeLa cells and (d) complex **6** in MCF-7 cells [symbols: black for dark and red for visible light (400–700 nm, 10 J cm^{-2})].

aip) ~ **2** (Fc-Trp-Cu-aip) > **1** (Ph-Tyr-Cu-aip) (Table 3, Fig. S18, ESI†). The complexes also showed photo-induced DNA cleavage activity in green light of 568 nm and red light of 647 nm with red light having the maximum tissue penetration. A 15 μmol solution of **4–6** essentially completely damaged plasmid DNA in red light for 2 h. Control experiments using the copper(ɪɪ) salts, the ferrocenyl amino acid reduced Schiff bases, aip or pyip alone did not show any apparent DNA photo-cleavage activity under similar reaction conditions (Fig. S19, ESI†).

Various inhibitors were used and their effects on the DNA cleavage activity were studied to elucidate the probable mechanism of the DNA cleavage by the complexes. The complexes were found to be ineffective under an argon atmosphere suggesting the involvement of oxygen dependent mechanistic pathways. The reactions were studied in blue and red light of 454 and 647 nm wavelengths using the complex **6** as a representative one and different additives (Fig. S20, ESI†). Singlet oxygen ($^1O_2$) quenchers, namely NaN₃, TEMP or L-His, did not show any significant inhibition in the cleavage reactions eliminating the possibility of a type-II pathway forming $^1O_2$ species. The hydroxyl radical scavengers, namely DMSO, KI and catalase, showed significant inhibition in the DNA cleavage activity. This suggests the formation of a hydroxyl radical *via* a photo-redox pathway. Superoxide dismutase (SOD) showed partial inhibition of the DNA photocleavage activity suggesting involvement of the superoxide radical anion which is known to dismutate at a very rapid rate forming ˙OH radicals.[60]

Cytotoxicity study

The *in vitro* photo-induced cytotoxicity of **1–10** was evaluated in human cervical carcinoma HeLa and human breast adeno-carcinoma MCF-7 cancer cells using the MTT (3-(4,5-dimethylthiazol-2-yl)-2,5-diphenyltetrazolium bromide) assay (Fig. 4, Table 4, Fig. S21–S23, ESI†). A dose-dependent anti-proliferative activity of the complexes was observed in both the cells. The complexes showed low dark toxicity owing to their redox inactivity at the copper(ɪɪ) centre. Photo-irradiation with a visible light of 400–700 nm, however, resulted in a significant enhancement in the cytotoxicity of the complexes, while the untreated control cells remained unaffected on light-exposure.
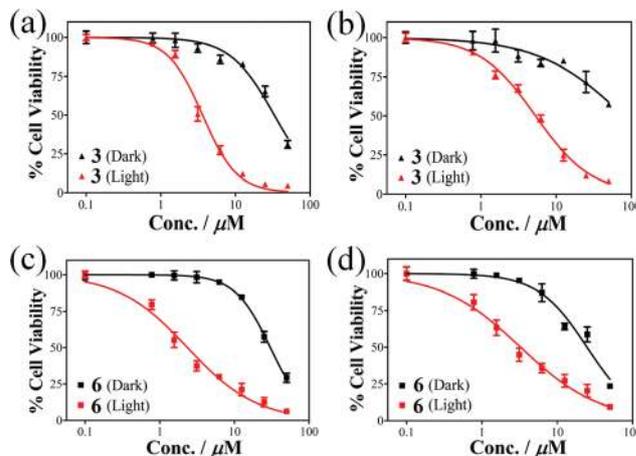
A remarkable increase of ~7–13 folds in cytotoxicity was observed for HeLa cells treated with the complex in visible light when compared to the non-irradiated samples. The complex **6** gave an IC₅₀ value of only 2.3 μmol in light while remaining non-toxic at a much higher concentration with an IC₅₀ value of ~30 μmol in the dark. To evaluate the role of the ferrocenyl moiety, phenyl analogues of the Fc-Met complexes **3** and **6** were tested for the photocytotoxic potential towards HeLa cells in visible light. The Ph-Met complexes **7** and **8** did not show any toxicity in HeLa cells under similar conditions to those used for **3** and **6**. The bis-imidazophenanthroline copper(ɪɪ) complexes, *viz.* [Cu(aip)₂(NO₃)](NO₃) (**9**) and [Cu-(pyip)₂(NO₃)](NO₃) (**10**), did not show any cytotoxicity upon photoactivation in visible light. This indicated the vital role played by the ferrocenyl moiety for induction of apoptosis in the cancer cells upon photo-excitation in visible light. The complexes **1–6** showed similar photo-enhanced anti-proliferative activity in MCF-7 cells. The IC₅₀ values in light were in the range of 3.2–6.1 μmol. Unlike most copper(ɪɪ) complexes, a very impressive dark *vs.* light profile was observed for both HeLa and MCF-7 cells. The pyrenyl imidazophenanthroline complexes **4–6** were found to be more cytotoxic probably due to their better cellular uptake and/or photo-activity. A comparison of the IC₅₀ values of the present complexes, Photofrin®, cisplatin and relevant copper(ɪɪ) complexes, is made in Table 4.[20,23,47] Complexes **1–6** are unique among the copper(ɪɪ) complexes in showing an unprecedented photocytotoxic effect possibly because of their unusual molecular structures with the axial site(s) blocked by the pendants thus making the copper(ɪɪ) centre redox inactive in a rigid structure (Fig. S13, ESI†). The observed photocytotoxicity is comparable to that of Photofrin®. Cisplatin that lacks any photoactive moiety gave an IC₅₀ value of ~70 μmol in both dark and light under similar assay conditions. The low dark toxicity and high photo-induced cytotoxicity make the present complexes potent candidates for photocytotoxic applications.

Table 4 The IC$_{50}$ values of Photofrin®, cisplatin, [Cu(Fc-aa)(aip)](ClO$_4$) (**1–3**), [Cu(Fc-aa)(pyip)](ClO$_4$) (**4–6**), controls and relevant copper(II) complexes in HeLa and MCF-7 cells

Compound	HeLa		MCF-7	
	IC$_{50}$ (μM) dark^a	IC$_{50}$ (μM) visible light^b	IC$_{50}$ (μM) dark^a	IC$_{50}$ (μM) visible light^b
[Cu(Fc-Tyr)(aip)](ClO$_4$) (**1**)	36.2 (±3.8)	4.8 (±0.4)	>50	5.9 (±0.8)
[Cu(Fc-Trp)(aip)](ClO$_4$) (**2**)	35.7 (±4.3)	4.3 (±0.4)	>50	6.1 (±0.7)
[Cu(Fc-Met)(aip)](ClO$_4$) (**3**)	33.1 (±4.1)	3.6 (±0.3)	>50	5.3 (±0.6)
[Cu(Fc-Tyr)(pyip)](ClO$_4$) (**4**)	29.3 (±2.5)	3.5 (±0.4)	27.0 (±4.3)	4.9 (±0.8)
[Cu(Fc-Trp)(pyip)](ClO$_4$) (**5**)	30.5 (±2.2)	3.3 (±0.5)	25.8 (±4.4)	4.3 (±0.5)
[Cu(Fc-Met)(pyip)](ClO$_4$) (**6**)	30.3 (±2.1)	2.3 (±0.3)	24.8 (±3.6)	3.2 (±0.5)
[Cu(Ph-Met)(aip)](ClO$_4$) (**7**)	>25	>25	—	—
[Cu(Ph-Met)(pyip)](ClO$_4$) (**8**)	>25	>25	—	—
[Cu(aip)$_2$(NO$_3$)](NO$_3$) (**9**)	>25	>25	—	—
[Cu(pyp)$_2$(NO$_3$)](NO$_3$) (**10**)	>25	11.9 (±1.1)	—	—
[Cu(Fc-Tyr)(dppz)](ClO$_4$)^c	2.31 (±0.19)	0.90 (±0.03)	2.7 (±0.3)	0.76 (±0.03)
[Cu(Fc-Tyr)(nip)](ClO$_4$)^c	4.07 (±0.16)	1.49 (±0.11)	5.73 (±0.31)	2.53 (±0.17)
[Cu(Fc-Trp)(dppz)](ClO$_4$)^d	8.95 (±0.20)	1.29 (±0.04)	2.99 (±0.08)	0.65 (±0.03)
[Cu(Fc-Met)(dppz)](NO$_3$)^e	2.61 (±0.16)	0.70 (±0.04)	4.08 (±0.39)	0.26 (±0.02)
[Cu(Fc-Met)(nip)](NO$_3$)^e	3.81 (±0.20)	1.54 (±0.13)	3.87 (±0.29)	1.37 (±0.21)
Photofrin®^{f}	>41	4.3 (±0.2)	—	—
Cisplatin^g	71.3 (±2.9)	68.7 (± 3.4)	—	—

^{a} The IC$_{50}$ values for the complexes **1–10** correspond to 4 h of incubation in the dark. ^{b} The IC$_{50}$ values correspond to 4 h of incubation in the dark followed by photo-exposure to visible light (400–700 nm, 10 J cm^{-2}). ^{c} The IC$_{50}$ values are taken from ref. 47a. Ligands dppz and nip are dipyridophenazine and naphthyl imidazophenanthroline, respectively. ^{d} The IC$_{50}$ values are taken from ref. 47b. ^{e} The IC$_{50}$ values are taken from ref. 47c. ^{f} Photofrin® IC$_{50}$ values (633 nm excitation; fluence rate: 5 J cm^{-2}) are taken from ref. 23. It is converted to μmol using the approximate molecular weight of Photofrin®, 600 g mol^{-1}. ^{g} The IC$_{50}$ values are taken from ref. 20 for 4 h of incubation. The IC$_{50}$ value is 7.2 μmol on 24 h of incubation in the dark.

Acridine orange–ethidium bromide dual staining

Acridine orange–ethidium bromide (AO–EB) dual staining was performed in HeLa cancer cells treated with complexes **3** and **6** to gain an insight into the mechanistic aspects of the cell death by looking at the changes in the nuclear morphology upon photo-exposure (Fig. 5, Fig. S24, ESI†). Of the two stains, only AO can cross the membrane to stain the DNA whereas EB is excluded. When cells undergo apoptosis, the membrane starts losing its integrity and during late apoptosis, cells take up EB and fluoresce red.[61] Cells treated with the complex in the dark did not show any significant change in the nuclear morphology and were evenly stained with AO and no EB staining (Fig. 5, panels (b) and (c)). But the HeLa cells treated with complexes **3** and **6** (10 and 20 μmol), upon photo-irradiation, showed a significant increase in the appearance of the apoptotic nuclear bodies wherein the nuclei had condensed, stained intensely with EB and the AO staining was low (Fig. 5, panels (e) and (f)). Cells cultured in the dark and the cells treated with DMSO showed negligible nuclear condensation and no EB staining (Fig. 5, panels (a) and (d)). The results indicate that the photo-irradiated cancer cells are in the late stage of apoptosis, and have lost membrane integrity, enabling ethidium bromide to enter the cells and staining the DNA.
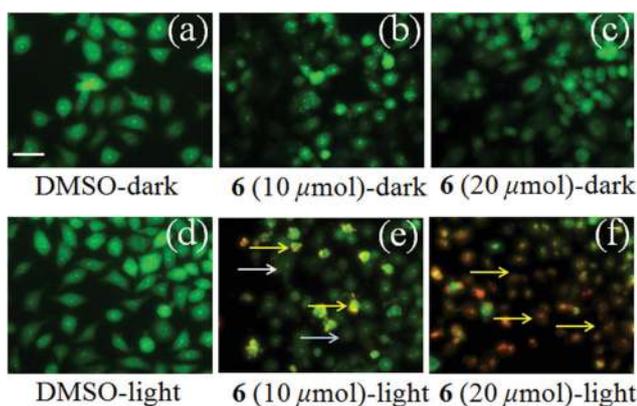

Fig. 5 Acridine orange (white arrow)–ethidium bromide (yellow arrow) (AO–EB) dual staining of the HeLa cells treated with the complex **6** (10 and 20 μmol) to study the nuclear morphology. Panels (a) and (d) correspond to the cells treated with only DMSO in the dark and light respectively, panels (b) and (c) correspond to the cells treated with the complex **6** in the dark. Panels (e) and (f) correspond to the cells treated with the complex **6** and irradiated with visible light (400–700 nm, 10 J cm^{-2}) [scale bar: 20 μm].

Cellular localization

The study on pharmacokinetics of an anticancer drug is of importance to understand its mode of action, localization in the cellular organelles and its target in the cellular medium.[62–64] Furthermore, imaging and therapeutic properties of a drug candidate are of importance to enhance its efficacy.[65–67] The present complexes are designed with pendant fluorescent anthracenyl and pyrenyl moieties emitting in blue to study their uptake and localization in the HeLa cells by fluorescence microscopy. Complexes **3** and **6** were used as two representative complexes for this purpose (Fig. 6, Fig. S25, ESI†). The fluorescence intensity was found to increase with time indicating an increased uptake of the complexes primarily in the cytosol of the HeLa cells even after 4 h time without
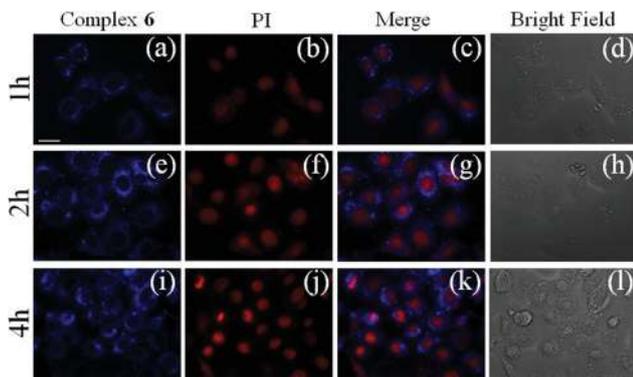
Fig. 6 A time-course collection of fluorescence microscopic images of HeLa cells treated with the complex **6** (10 μmol) and propidium iodide (PI). Panels (a), (e) and (i) correspond to the blue emission of the complex **6** and the respective images were taken after 1, 2 and 4 h. Panels (b), (f) and (j) correspond to the red emission of PI. Panels (c), (g) and (k) show the merged images of the first two panels. Panels (d), (h) and (l) show the bright field images. The scale bar in the panels corresponds to 20 μm.

any significant nuclear uptake (Fig. 6, panels (a), (e) and (i)). The cells were stained with propidium iodide (PI), which stains only the nucleus, in the presence of RNase by degrading the cellular RNA (Fig. 6, panels (b), (f) and (j)). The merged images do not show any nuclear localization of the complexes and preferential localization in the cytosol of the HeLa cells was observed (Fig. 6, panels (c), (g) and (k)). Cytosolic localization is preferred in PDT than nuclear localization to prevent any unwanted mutation of the nuclear DNA.

Further studies were carried out to see if there is any selectivity in cytosolic localization. Despite being in the cytosol, the complexes appeared more punctate in their localization (Fig. 7), indicating possible localization in particular organelles within the cells. To understand the same, HeLa cells were treated with the complex **6** for different time intervals followed by staining two specific organelles, namely the endo-
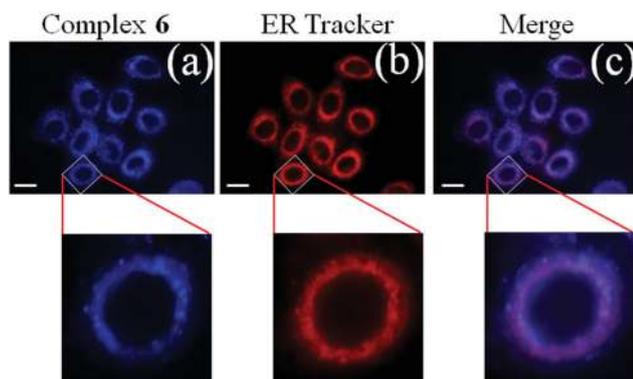
Fig. 7 Fluorescence microscopic images of HeLa cells treated with the complex **6** (10 μmol) and endoplasmic reticulum (ER) Tracker Red. Panels (a), (b) and (c) correspond to the blue emission of complex **6**, red emission of ER Tracker Red and the merged images respectively taken after 4 h. Enlarged images are shown at the bottom. The scale bar in the panels corresponds to 20 μm.

plasmic reticulum (ER) and the mitochondria, which form distinct punctate structures in the cells. Fluorescence microscopy of these cells showed predominant co-localization of the complex with the ER Tracker Red that was used to mark the ER, indicating selective localization of the complex in the ER (Fig. 7, panels (a)–(c), Fig. S26 and S27, ESI†). The localization did not change with time, although by 4 h, some of the complex started diffusing to areas outside the ER, to the cytosol (Fig. 7, panels (a)–(c)). Staining of cells, treated with the complex **6**, with MitoTracker Red indicated that the complex barely localized to the mitochondria after 1 h of treatment. Further analysis with MitoTracker was found to be difficult as both the tracker and the complex started diffusing out indicating a possible charge based competition between the complex and the tracker (Fig. S28, ESI†). Furthermore, to study whether incorporation of the ferrocenyl moiety makes any difference in the localization behavior of the complexes, the control complexes were tested for their localization in HeLa cells in the presence of the ER tracker. The Ph-Met and the bis-imidazo-phenanthroline complexes showed similar localization behavior, although more diffused compared to the ferrocenyl complexes, in HeLa cells (Fig. S29 and S30, ESI†). This implies that the difference in cellular activities of the ferrocenyl complexes with their non-ferrocenyl analogues is probably not due to their localization behavior, but based on their abilities to generate cytotoxic species upon photo-activation with visible light.

Conclusion

The ferrocene-conjugated ʟ-amino acid reduced Schiff base (Fc-Tyr, Fc-Trp and Fc-Met) copper(ɪɪ) complexes containing imidazophenanthroline derivatives having the anthracenyl or pyrenyl moiety were designed and synthesized as new bioorganometallics showing remarkable photocytotoxic activity in visible light. Incorporation of the ferrocenyl moiety conjugated to a copper(ɪɪ) center through a reduced Schiff base linker provided a broader spectral range of excitation to achieve the desired photoactivity. The presence of the fluorescent anthracenyl and pyrenyl moieties as pendants to the phenanthroline bases allows imaging of the cells to study localization of the complexes in the cellular medium. The aromatic π-system of the complexes makes them excellent binders to ct-DNA with an intercalative mode of DNA binding. Unlike most copper(ɪɪ) complexes the present ones were chemical nuclease inactive in the presence of both reducing and oxidizing agents. The complexes, however, displayed significant photo-induced DNA cleavage activity in blue, green and red light. The complexes showed remarkable photocytotoxicity in HeLa and MCF-7 cancer cells with low dark toxicity because of the presence of the redox inactive copper(ɪɪ) center. The PDT efficacy of the complexes is comparable to that of the FDA approved drug Photofrin®. The evaluation of the photocytotoxic potential of the non-ferrocenyl control complexes clearly demonstrates the need for the ferrocenyl moiety to achieve remarkable photo-

cytotoxicity in low energy visible light. The AO–EB dual staining indicated significant morphological changes in the HeLa cells treated with the test complexes. Fluorescence microscopy showed the complexes primarily localizing in the cytosol of the HeLa cells as is known for the porphyrinic drug Photofrin®. The novel aspect of this work is the observation of the complex localizing specifically in the endoplasmic reticulum. This work exemplifies a new class of metal-based PDT agents that are excellent DNA binders, efficient photocleavers of DNA and photocytotoxic agents which are capable of localizing in the cytosol, particularly in the endoplasmic reticulum (ER), of the cancer cells thus minimizing the possibility of having any mutation of nuclear DNA on photoactivation.

Experimental

Materials and methods

All the reagents and chemicals were obtained from commercial sources (S.D. Fine Chemicals, India; Sigma-Aldrich, U.S.A.) and were used as such. Solvents used were purified by reported procedures.[68] Supercoiled pUC19 DNA (cesium chloride purified) was purchased from Bangalore Genie (India). Tris-(hydroxymethyl)aminomethane–HCl (Tris-HCl) buffer solution of pH 7.2 was prepared using deionized and sonicated triple distilled water. 9-Anthraldehyde, 1-pyrene-carboxaldehyde, calf thymus (ct) DNA, agarose (molecular biology grade), KI, catalase, NaN_3, L-histidine, SOD (superoxide dismutase), 2,2,6,6-tetramethyl-4-piperidone (TEMP), acridine orange (AO), ethidium bromide (EB), bromophenol blue, xylene cyanol, Dulbecco's modified Eagle's medium (DMEM), propidium iodide (PI) and MTT (3-(4,5-dimethylthiazol-2-yl)-2,5-diphenyltetrazolium bromide) were purchased from Sigma (U.S.A.). ER-Tracker Red and MitoTracker Red were bought from Invitrogen (U.S.A.). 2-(9-Anthryl)-1H-imidazo[4,5-f][1,10]phenanthroline (aip) and 2-(1-pyrenyl)-1H-imidazo[4,5-f][1,10]phenanthroline (pyip) were prepared following a literature procedure using 1,10-phenanthroline-5,6-dione and 9-anthraldehyde or 1-pyrene-carboxaldehyde in the presence of ammonium acetate and glacial acetic acid.[53] Ligands Fc-MetH, Ph-MetH, Fc-TrpH and Fc-TyrH were prepared following literature procedures (Fig. S1–S4†).[69,70]

The elemental analysis was carried out using a Thermo Finnigan Flash EA 1112 CHN analyzer. The infrared and electronic spectra were recorded on Perkin-Elmer Lambda 35 and Perkin-Elmer Spectrum one 55 spectrophotometers, respectively. ^{1}H NMR spectra were recorded at room temperature using a Bruker 400 MHz NMR spectrometer. Molar conductivity measurements were performed using a Control Dynamics (India) conductivity meter. Room temperature magnetic susceptibilities of the ferrocenyl copper(II) complexes in DMSO-d_6 solution containing 1% TMS (v/v) as the internal reference were obtained by the Evans method using a Bruker AMX-400 NMR spectrometer.[71,72] The magnetic moments were calculated using the equation: $\mu_{eff} = 0.0618((\Delta f)T/fM)$, where Δf is the observed shift in the frequency of the TMS signal, T is the

temperature (K), f is the operating frequency (MHz) of the NMR spectrometer and M is the molarity of the complex in the solution. Cyclic voltammetric measurements were made at 25 °C using a EG&G PAR Model 253 VersaStat potentiostat/galvanostat using a three electrode set-up comprising of a glassy carbon working electrode, a platinum wire auxiliary electrode and a saturated calomel reference (SCE) electrode. Tetrabutylammonium perchlorate (TBAP) (0.1 mol) was used as a supporting electrolyte in DMF. The electrochemical data were uncorrected for junction potentials. Electrospray ionization mass spectral measurements were performed using an Esquire 3000 plus ESI (Bruker Daltonics) Spectrometer. The experimental and calculated ESI-MS values for each complex were identical to a significant last figure above the decimal point.

Synthesis

Preparation of [Cu(Fc-aa)(aip)](ClO$_4$) (Fc-aa = Fc-Tyr in 1, Fc-Trp in 2, Fc-Met in 3). Complexes **1–3** were prepared by a general synthetic procedure in which 0.2 g (1.0 mmol) of copper(II) acetate monohydrate in methanol was reacted with a methanol solution of 2-(9-anthryl)-1H-imidazo[4,5-f][1,10]phenanthroline (aip, 0.29 g; 1.0 mmol) while stirring at room temperature for 1 h followed by addition of the solid Fc-aaH (Fc-aaH: Fc-TyrH, 0.38 g; Fc-TrpH, 0.40 g; Fc-MetH, 0.35 g, 1.0 mmol) in small portions with continuous stirring. The reaction mixture was stirred for 2 h and the product was precipitated on addition of a methanol solution of $NaClO_4$ (1.0 mmol, 0.12 g). The product was washed with water, cold methanol, diethyl ether and finally dried in a vacuum over P_4O_{10} to obtain a pale green solid in ~80% yield (yield: 0.73 g, 78% for **1**; 0.77 g, 80% for **2**; 0.74 g, 81% for **3**) (Scheme S1, ESI†).

Anal. Calcd for $C_{47}H_{36}N_5O_7ClFeCu$ (**1**): C, 59.56; H, 4.89; N, 7.39. Found: C, 59.31; H, 4.73; N, 7.65. Selected IR data (cm^{-1}): 3470br, 2927w, 1639vs (COO_{asym}), 1552w, 1512m, 1442m, 1410m, 1360s (COO_{sym}), 1310w, 1247w, 1085vs (ClO_4^{-}), 1050w, 898w, 810s, 726vs, 621s, 552w, 483s, 428m (vs, very strong; s, strong; m, medium; w, weak; br, broad). ESI-MS in MeOH: m/z 837 $[M - (ClO_4^{-})]^{+}$. UV-visible in DMF–Tris-HCl buffer (1:1 v/v) [λ_{max}/nm (ε/dm^3 mol^{-1} cm^{-1})]: 605 (145), 386 (8750), 371 (9225), 352 (7960), 264sh (58 490), 254 (86 230). μ_{eff} = 1.82μ_B at 298 K. Λ_M = 85 S m^2 mol^{-1} in DMF at 25 °C.

Anal. Calcd for $C_{49}H_{47}N_6O_6ClFeCu$ (**2**): C, 60.62; H, 4.88; N, 8.66. Found: C, 60.35; H, 4.92; N, 8.49. Selected IR data (cm^{-1}): 3472br, 2921w, 1643vs (COO_{asym}), 1552w, 1507w, 1442m, 1411m, 1359s (COO_{sym}), 1340w, 1308w, 1250w, 1185w, 1085vs (ClO_4^{-}), 900w, 810s, 738vs, 621s, 481s, 428m. ESI-MS in MeOH: m/z 860 $[M - (ClO_4^{-})]^{+}$. UV-visible in DMF–Tris-HCl buffer (1:1 v/v) [λ_{max}/nm (ε/dm^3 mol^{-1} cm^{-1})]: 600 (150), 386 (8300), 371 (8785), 352 (7715), 264sh (62 990), 254 (82 680). μ_{eff} = 1.80μ_B at 298 K. Λ_M = 83 S m^2 mol^{-1} in DMF at 25 °C.

Anal. Calcd for $C_{43}H_{36}N_5O_6SClFeCu$ (**3**): C, 57.02; H, 4.01; N, 7.73. Found: C, 56.75; H, 4.10; N, 7.87. Selected IR data (cm^{-1}): 3067br, 2921w, 1638vs (COO_{asym}), 1556w, 1506w, 1441m, 1409m, 1359s (COO_{sym}), 1310m, 1251w, 1188w, 1087vs (ClO_4^{-}), 894m, 810s, 729vs, 621s, 482s, 427m. ESI-MS in

MeOH: m/z 805 $[M - (ClO_4^-)]^+$. UV-visible in DMF–Tris-HCl buffer (1 : 1 v/v) $[\lambda_{max}/nm\ (\varepsilon/dm^3\ mol^{-1}\ cm^{-1})]$: 600 (135), 386 (7905), 371 (8360), 352 (7155), 264sh (55 250), 254 (75 660). μ_{eff} = 1.79μ_B at 298 K. Λ_M = 79 S m^2 mol^{-1} in DMF at 25 °C.

Preparation of [Cu(Fc-aa)(pyip)](ClO$_4$) (Fc-aa = Fc-Tyr in 4, Fc-Trp in 5, Fc-Met in 6). Complexes **4–6** were prepared following a similar procedure to that described for **1–3** (1.0 mmol scale) using 2-(1-pyrenyl)-1H-imidazo[4,5-f][1,10]phenanthroline (pyip) instead of aip. A greenish brown solid was isolated on addition of a methanolic solution of NaClO$_4$. The solid was washed with water, cold methanol, diethyl ether and finally dried *in vacuo* over P$_4$O$_{10}$ to obtain the product in ~85% yield (yield: 0.8 g, ~83% for **4**, 0.85 g, ~86% for **5**, 0.79 g, ~85% for **6**) (Scheme S1, ESI†).

Anal. Calcd for C$_{49}$H$_{36}$N$_5$O$_7$ClFeCu (**4**): C, 61.20; H, 3.77; N, 7.28. Found: C, 60. 93; H, 4.01; N, 7.44. Selected IR data (cm^{-1}): 3085br, 2924w, 1630vs (COO$_{asym}$), 1507w, 1455m, 1435m, 1410m, 1360s (COO$_{sym}$), 1230m, 1202w, 1095vs (ClO$_4^-$), 1000m, 914w, 848m, 810s, 741vs, 662w, 621s, 532w, 481s, 428m. ESI-MS in MeOH: m/z 861 $[M - (ClO_4^-)]^+$. UV-visible in DMF–Tris-HCl buffer (1 : 1 v/v) $[\lambda_{max}/nm\ (\varepsilon/dm^3\ mol^{-1}\ cm^{-1})]$: 615 (140), 400 (18 260), 372 (21 710), 288 (31 490), 277 (29 510), 244 (43 950). μ_{eff} = 1.81μ_B at 298 K. Λ_M = 78 S m^2 mol^{-1} in DMF at 25 °C.

Anal. Calcd for C$_{51}$H$_{37}$N$_6$O$_6$ClFeCu (**5**): C, 62.21; H, 3.79; N, 8.53. Found: C, 62.01; H, 3.91; N, 8.37. Selected IR data (cm^{-1}): 3085br, 2921w, 1626vs (COO$_{asym}$), 1506m, 1458m, 1430m, 1409m, 1359s (COO$_{sym}$), 1227m, 1095vs (ClO$_4^-$), 995w, 904w, 848m, 414s, 736s, 659w, 617s, 575w, 533w, 477s, 428m. ESI-MS in MeOH: m/z 884 $[M - (ClO_4^-)]^+$. UV-visible in DMF–Tris-HCl buffer (1 : 1 v/v) $[\lambda_{max}/nm\ (\varepsilon/dm^3\ mol^{-1}\ cm^{-1})]$: 615 (130), 400 (12 960), 372 (15 070), 288 (19 140), 277 (28 950), 247 (34 935). μ_{eff} = 1.78μ_B at 298 K. Λ_M = 82 S m^2 mol^{-1} in DMF at 25 °C.

Anal. Calcd for C$_{45}$H$_{36}$N$_5$O$_6$SClFeCu (**6**): C, 58.13; H, 3.90; N, 7.53. Found: C, 57.88; H, 4.09; N, 7.31. Selected IR data (cm^{-1}): 3482br, 2914w, 1626vs (COO$_{asym}$), 1506w, 1443m, 1409m, 1359s (COO$_{sym}$), 1310w, 1227w, 1090vs (ClO$_4^-$), 904w, 848m, 807s, 723s, 627s, 477s, 428m. ESI-MS in MeOH: m/z 829 $[M - (ClO_4^-)]^+$. UV-visible in DMF–Tris-HCl buffer (1 : 1 v/v) $[\lambda_{max}/nm\ (\varepsilon/dm^3\ mol^{-1}\ cm^{-1})]$: 620 (140), 400 (17 490), 372 (22 510), 288 (30 185), 277 (29 915), 244 (41 930). μ_{eff} = 1.77μ_B at 298 K. Λ_M = 79 S m^2 mol^{-1} in DMF at 25 °C.

Preparation of [Cu(Ph-Met)(aip)](ClO$_4$) (7) and [Cu(Ph-Met)(pyip)](ClO$_4$) (8). Complexes **7** and **8** were prepared following a similar procedure to that described for **1–3** and **4–6**, respectively, and isolated as a pale green solid (yield: 74% for **7**; 70% for **8**) (Scheme S2, ESI†).

Preparation of [Cu(aip)$_2$(NO$_3$)](NO$_3$) (9) and [Cu(pyip)$_2$(NO$_3$)](NO$_3$) (10). Complexes **9** and **10** were prepared by following a general procedure in which 0.24 g (1.0 mmol) of copper(II) nitrate trihydrate in methanol was reacted with a methanol solution of 2-(9-anthryl)-1H-imidazo[4,5-f][1,10]phenanthroline (0.58 g; 2.0 mmol) or 2-(1-pyrenyl)-1H-imidazo[4,5-f][1,10]phenanthroline (0.84 g, 2.0 mmol) at room temperature. The reaction mixture was stirred for 2 h and the product was isolated by concentration of the reaction mixture and recrystallization was done from methanol. The product was washed with water, cold methanol, and diethyl ether and finally dried in a vacuum over P$_4$O$_{10}$ to obtain a pale green solid (yield: 76% for **9**; 68% for **10**) (Scheme S3, ESI†)

CAUTION! The perchlorate salts being potentially explosive, only small quantities of the complexes were handled with precautions.

Solubility and stability

The complexes were soluble in MeOH, DMF, DMSO, MeCN and in the aqueous mixtures of these solvents; less soluble in CHCl$_3$ and CH$_2$Cl$_2$, and insoluble in hydrocarbon solvents. They were stable in both solid and solution phases.

Computational methodology

The geometries of the complexes were optimized by the DFT method using Gaussian 03.[54] The B3LYP functional was used for the calculation by employing two types of basis sets, *viz.* 6-31G for lighter elements (C, N, H, O and S) and LanL2DZ for the heavier elements (Fe and Cu).[55]

DNA binding and cleavage experiments

The DNA binding and cleavage experiments were carried out using calf thymus (ct) DNA and supercoiled (SC) pUC19 DNA, respectively, by following reported procedures.[73] For UV-visible absorption titration, Tris-HCl buffer of pH 7.2 was used and the ct-DNA concentration was 235 µmol. DNA thermal denaturation experiments were carried out in phosphate buffer (pH 6.8) using 200 µmol ct-DNA and 20 µmol complexes by varying the temperature from 40 to 90 °C. The ratio of the complex and DNA concentration was 1 : 10. DNA viscometric titrations were performed in Tris-HCl buffer using 160 µmol ct-DNA. The SC pUC19 DNA cleavage activity of the complexes **1–6** was studied in blue, green and red light of 454, 568 and 647 nm wavelengths using a Spectra Physics Water-Cooled Mixed-Gas Ion Laser Stabilite® 2018-RM (continuous-wave (CW) beam diameter at 1/e^2 = 1.8 mm ± 10% and beam divergence with full angle = 0.7 mrad ± 10%, laser power = 50 mW) and in the dark. The chemical nuclease activity of the complexes was studied using external additives like glutathione (GSH) and hydrogen peroxide (H$_2$O$_2$). Mechanistic investigations were carried out using various singlet oxygen quenchers and radical scavengers to detect formation of any reactive oxygen species (ROS).

Cell culture

HeLa (human cervical carcinoma) and MCF-7 (human breast adenocarcinoma) cells were maintained in Dulbecco's modified Eagle's medium (DMEM), supplemented with 10% fetal bovine serum (FBS), 100 IU ml^{-1} of penicillin, 100 µg ml^{-1} of streptomycin and 2 mmol Glutamax at 37 °C in a humidified incubator at 5% CO$_2$. The adherent cultures were grown as monolayers and were passaged once in 4–5 days by treatment with 0.25% Trypsin-EDTA.

Cell viability assay

HeLa and MCF-7 cancer cells were analyzed for viability post-treatment using the MTT assay. The photocytotoxicity of the complexes was based on the ability of mitochondrial dehydrogenases in the viable cells to cleave the tetrazolium rings of MTT to form dark blue membrane impermeable crystals of formazan that were measured at 540 nm giving an estimate of the number of viable cells.[74] Approximately 15×10^3 HeLa cells or 2×10^4 MCF-7 cells were plated in a 96-well culture plate in DMEM supplemented with 10% fetal bovine serum (10% FBS) and cultured overnight. Different concentrations of the complexes were added to the cells, and incubation was continued for 4 h in the dark. After incubation, the medium was replaced with 50 mmol phosphate buffer (pH 7.4) containing 150 mmol NaCl (PBS) and cells were photo-irradiated for 1 h in visible light of 400–700 nm using a Luzchem Photoreactor (Model LZC-1, Ontario, Canada; light fluence rate: 2.4 mW cm^{-2}; light dose = 10 J cm^{-2}). PBS was replaced with 10% DMEM after irradiation and cells were incubated for a further period of 20 h in the dark. Post incubation, 25 μl of MTT (4 mg ml^{-1} of PBS) was added to each well and incubated for an additional 3 h. The culture medium was discarded and 200 μl of DMSO was added to dissolve the formazan crystals. The intensity of the dark blue color formed by the formazan complex was read at an absorbance of 540 nm using an ELISA microplate reader (BioRad, Hercules, CA, USA). The cytotoxicity of the test compounds was measured as the percentage ratio of the absorbance of the treated cells over the untreated controls. The IC$_{50}$ values were determined by nonlinear regression analysis (GraphPad Prism).

Cell death analysis by dual staining

HeLa cells (4×10^4 cells mm^{-2}) cultured on cover slips were photo-irradiated with visible light of 400–700 nm (light fluence rate = 2.4 mW cm^{-2}; light dose = 10 J cm^{-2}) following 4 h of incubation in the dark in the presence of 10 and 20 μmol of complexes **3** and **6**. The cells were then allowed to recover for 2 h, washed three times with PBS and stained with the acridine orange–ethidium bromide (AO–EB) mixture (1 : 1, 10 μmol) for 15 min and observed at 20× magnification with a fluorescence microscope (Carl Zeiss). The images were analyzed using the "Image J" image browser.[75]

Fluorescence microscopy

HeLa cells (4×10^4 cells mm^{-2}) were incubated with complexes **3**, **6**, **7–10** (10 μmol) with time intervals 1 to 4 h in the dark and fixed with 4% paraformaldehyde for 10 min at 25 °C and washed with PBS. This was followed by incubation with PI staining solution (50 μg ml^{-1} RNase A, 20 μg ml^{-1} PI in PBS) for 1 h at 42 °C. The cells were washed free of excess PI and mounted in 90% glycerol solution containing Mowiol, an anti-fade reagent, and sealed. Images acquired using an Apotome.2 fluorescence microscope (Carl Zeiss, Germany) using an oil immersion lens at 63× magnification were analyzed using the AxioVision Rel 4.8.2 (Carl Zeiss, Germany) software.[76]

To understand the sub-cellular localization of the complexes, HeLa cells (4×10^4 cells mm^{-2}) were incubated with 10 μmol of the complex **6** for different time intervals from 1 to 4 h in the dark, following which, the cells were treated with 0.5 μmol of ER-Tracker Red or 0.25 μmol MitoTracker Red in serum-free medium for 20–30 min at 37 °C. The cells were then washed with PBS, mounted on slides and sealed. The images were acquired using the Apotome.2 fluorescence microscope at 63× magnification and analyzed using AxioVision Rel 4.8.2 for sub-cellular localization of the compound.

Acknowledgements

Notes and references

1 R. Bonnett, *Chemical Aspects of Photodynamic Therapy*, Gordon & Breach, London, U.K., 2000.

2 T. D. Maurer, B. J. Kraft, S. M. Lato, A. D. Ellington and J. M. Zaleski, *Chem. Commun.*, 2000, 69–70.

3 (*a*) N. L. Fry and P. K. Mascharak, *Acc. Chem. Res.*, 2011, **44**, 289–298; (*b*) U. Schatzschneider, *Inorg. Chim. Acta*, 2011, **374**, 19–23.

4 M. J. Rose, N. L. Fry, R. Marlow, L. Hinck and P. K. Mascharak, *J. Am. Chem. Soc.*, 2008, **130**, 8834–8846.

5 A. D. Ostrowski and P. C. Ford, *Dalton Trans.*, 2009, 10660–10669.

6 D. Crespy, K. Landfester, U. S. Schubert and A. Schiller, *Chem. Commun.*, 2010, **46**, 6651–6662.

7 H. T. Chifotides and K. R. Dunbar, *Acc. Chem. Res.*, 2005, **38**, 146–156.

8 A. M. Angeles-Boza, H. T. Chifotides, J. D. Aguirre, A. Chouai, P. K.-L. Fu, K. R. Dunbar and C. Turro, *J. Med. Chem.*, 2006, **49**, 6841–6847.

9 R. Zhao, R. Hammitt, R. P. Thummel, Y. Liu, C. Turro and R. M. Snapka, *Dalton Trans.*, 2009, 10926–10931.

10 N. J. Farrer, L. Salassa and P. J. Sadler, *Dalton Trans.*, 2009, 10690–10701.

11 N. J. Farrer and P. J. Sadler, *Aust. J. Chem.*, 2008, **61**, 669–674.

12 U. Schatzschneider, *Eur. J. Inorg. Chem.*, 2010, 1451–1467.

13 S. L. H. Higgins, A. J. Tucker, B. S. J. Winkel and K. J. Brewer, *Chem. Commun.*, 2012, **48**, 67–69.

14 M. Brindell, E. Kuliś, S. K. Elmroth, K. Urbańska and G. Stochel, *J. Med. Chem.*, 2005, **48**, 7298–7304.

15 F. S. Mackay, J. A. Woods, P. Heringová, J. Kašpárková, A. M. Pizarro, S. A. Moggach, S. Parsons, V. Brabec and P. J. Sadler, *Proc. Natl. Acad. Sci. U. S. A.*, 2007, **104**, 20743–22074.

16 P. K. Sasmal, S. Saha, R. Majumdar, R. R. Dighe and A. R. Chakravarty, *Chem. Commun.*, 2009, 1703–1705.

17 S. Banerjee, A. Hussain, P. Prasad, I. Khan, B. Banik, P. Kondaiah and A. R. Chakravarty, *Eur. J. Inorg. Chem.*, 2012, 3899–3908.

18 U. Basu, I. Khan, A. Hussain, P. Kondaiah and A. R. Chakravarty, *Angew. Chem., Int. Ed.*, 2012, **51**, 2658–2661.

19 S. Saha, R. Majumdar, M. Roy, R. R. Dighe and A. R. Chakravarty, *Inorg. Chem.*, 2009, **48**, 2652–2663.

20 S. Saha, D. Mallick, R. Majumdar, M. Roy, R. R. Dighe, E. D. Jemmis and A. R. Chakravarty, *Inorg. Chem.*, 2011, **50**, 2975–2987.

21 (*a*) M. Ochsner, *J. Photochem. Photobiol., B*, 1996, **32**, 3–9; (*b*) S. I. Moriwaki, J. Misawa, Y. Yoshinari, I. Yamada, M. Takigawa and Y. Tokura, *Photodermatol. Photoimmunol. Photomed.*, 2001, **17**, 241–243.

22 C. J. Burrows and J. G. Muller, *Chem. Rev.*, 1998, **98**, 1109–1151.

23 E. Delaey, F. Van Larr, D. De Vos, A. Kamuhabwa, P. Jacobs and P. De Witte, *J. Photochem. Photobiol., B*, 2000, **55**, 27–36.

24 J. Saczko, M. Mazurkiewicz, A. Chwilkowska, J. Kulbacka, G. Kramer, M. Ługowski, M. Śnietura and T. Banas, *Folia Biol.*, 2007, **53**, 7–12.

25 S. Wang and R. J. Kaufman, *J. Cell Biol.*, 2012, **197**, 857–867.

26 S. Shen, Y. Zhang, R. Zhang and X. Gong, *Biochem. Biophys. Res. Commun.*, 2013, **15**, 519–524.

27 T. Verfaillie, A. D. Garg and P. Agostinis, *Cancer Lett.*, 2013, **332**, 249–264.

28 S. E. Logue, P. Cleary, S. Saveljeva and A. Samali, *Apoptosis*, 2013, **18**, 537–546.

29 S. Banerjee, A. Dixit, R. N. Shridharan, A. A. Karande and A. R. Chakravarty, *Chem. Commun.*, 2014, **50**, 5590–5592.

30 C. G. Hartinger and P. J. Dyson, *Chem. Soc. Rev.*, 2009, **38**, 391–401.

31 C. G. Hartinger, N. Metzler-Nolte and P. J. Dyson, *Organometallics*, 2012, **31**, 5677–5685.

32 A. F. A. Peacock and P. J. Sadler, *Chem. – Asian J.*, 2008, **3**, 1890–1899.

33 G. Gasser, I. Ott and N. Metzler-Nolte, *J. Med. Chem.*, 2011, **54**, 3–25.

34 M. F. R. Fouda, M. M. Abd-Elzaher, R. A. Abdelsamaia and A. A. Labib, *Appl. Organomet. Chem.*, 2007, **21**, 613–625.

35 J. é. Debreczeni, A. N. Bullock, G. E. Atilla, D. S. Williams, H. Bregman, S. Knapp and E. Meggers, *Angew. Chem., Int. Ed.*, 2006, **45**, 1580–1585.

36 Y. K. Yan, M. Melchart, A. Habtemariam and P. J. Sadler, *Chem. Commun.*, 2005, 4764–4776.

37 C. Ornelas, *New J. Chem.*, 2011, **35**, 1973–1985.

38 B. Maity and A. R. Chakravarty, *Indian J. Chem., Sec A: Inorg., Bio-inorg., Phys., Theor. Anal. Chem.*, 2012, **51**, 69–82.

39 A. Nguyen, S. Top, A. Vessieres, P. Pigeon, M. Huche, E. A. Hillard and G. Jaouen, *J. Organomet. Chem.*, 2007, **692**, 1219–1225.

40 F. Schmitt, P. Govindaswamy, G. Süss-Fink, W. H. Ang, P. J. Dyson, L. Juillerat-Jeanneret and B. Therrien, *J. Med. Chem.*, 2008, **51**, 1811–1816.

41 F. Schmitt, P. Govindaswamy, O. Zava, G. Süss-Fink, L. Juillerat-Jeanneret and B. Therrien, *J. Biol. Inorg. Chem.*, 2009, **14**, 101–109.

42 B. Balaji, B. Banik, P. K. Sasmal, B. Maity, R. Majumdar, R. R. Dighe and A. R. Chakravarty, *Eur. J. Inorg. Chem.*, 2012, 126–135.

43 B. Maity, M. Roy, B. Banik, R. Majumdar, R. R. Dighe and A. R. Chakravarty, *Organometallics*, 2010, **29**, 3632–3641.

44 B. Maity, S. Gadadhar, T. K. Goswami, A. A. Karande and A. R. Chakravarty, *Dalton Trans.*, 2011, **40**, 11904–11913.

45 B. Maity, M. Roy, S. Saha and A. R. Chakravarty, *Organometallics*, 2009, **28**, 1495–1505.

46 T. K. Goswami, M. Roy, M. Nethaji and A. R. Chakravarty, *Organometallics*, 2009, **28**, 1992–1994.

47 (*a*) T. K. Goswami, S. Gadadhar, A. A. Karande and A. R. Chakravarty, *Polyhedron*, 2013, **52**, 1287–1298; (*b*) T. K. Goswami, B. V. S. K. Chakravarthi, M. Roy, A. A. Karande and A. R. Chakravarty, *Inorg. Chem.*, 2011, **50**, 8452–8464; (*c*) T. K. Goswami, S. Gadadhar, M. Roy, M. Nethaji, A. A. Karande and A. R. Chakravarty, *Organometallics*, 2012, **31**, 3010–3021.

48 P. U. Maheswari, M. van der Ster, S. Smulders, S. Barends, G. P. van Wezel, C. Massera, S. Roy, H. den Dulk, P. Gamez and J. Reedijk, *Inorg. Chem.*, 2008, **47**, 3719–3727.

49 R. Loganathan, S. Ramakrishnan, E. Suresh, A. Riyasdeen, M. A. Akbarsha and M. Palaniandavar, *Inorg. Chem.*, 2012, **51**, 5512–5532.

50 T. Zou, C.-N. Lok, Y. M. E. Fung and C.-M. Che, *Chem. Commun.*, 2013, **49**, 5423–5425.

51 Y. Liu and Y. Ye, *Cell Res.*, 2011, **21**, 867–883.

52 M. Kurtoglu, K. Philips, H. Liu, L. H. Boise and T. J. Lampidis, *Cancer Chemother. Pharmacol.*, 2010, **66**, 129–140.

53 M. Mariappan and B. G. Maiya, *Eur. J. Inorg. Chem.*, 2005, 2164–2173.

54 M. J. Frisch, G. W. Trucks, H. B. Schlegel, G. E. Scuseria, M. A. Robb, J. R. Cheeseman, J. A. Montgomery, T. Vreven, K. N. Kudin, J. C. Burant, J. M. Millam, S. S. Iyengar, J. Tomasi, V. Barone, B. Mennucci, M. Cossi, G. Scalmani, N. Rega, G. A. Petersson, H. Nakatsuji, M. Hada, M. Ehara, K. Toyota, R. Fukuda, J. Hasegawa, H. Ishida, T. Nakajima, Y. Honda, O. Kitao, H. Nakai, M. Klene, X. Li, J. E. Knox, H. P. Hratchian, J. B. Cross, C. Adamo, J. Jaramillo, R. Gomperts, R. E. Stratmann, O. Yazyev, A. J. Austin, R. Cammi, C. Pomelli, J. Ochterski, P. Y. Ayala, K. Morokuma, G. A. Voth, P. Salvador, J. J. Dannenberg, V. G. Zakrzewski, S. Dapprich, A. D. Daniels, M. C. Strain, O. Farkas, D. K. Malick, A. D. Rabuck, K. Raghavachari, J. B. Foresman, J. V. Ortiz, Q. Cui, A. G. Baboul, S. Clifford, J. Cioslowski, B. B. Stefanov, G. Liu, A. Liashenko,

P. Piskorz, I. Komaromi, R. L. Martin, D. J. Fox, T. Keith, M. A. Al-Laham, C. Y. Peng, A. Nanayakkara, M. Challacombe, P. M. W. Gill, B. Johnson, W. Chen, M. W. Wong, C. Gonzalez and J. A. Pople, *Gaussian 03, revision B.4*, Gaussian Inc., Pittsburgh, PA, 2003.

55 A. D. Becke, *J. Chem. Phys.*, 1993, **98**, 5648–5652.

56 A. M. Pyle, J. P. Rehmann, R. Meshoyrer, C. V. Kumar, N. J. Turro and J. K. Barton, *J. Am. Chem. Soc.*, 1989, **111**, 3051–3058.

57 M. Cory, D. D. Mckee, J. Kagan, D. W. Henry and J. A. Miller, *J. Am. Chem. Soc.*, 1985, **107**, 2528–2536.

58 K. E. Reinert, *Biochim. Biophys. Acta*, 1973, **319**, 135–139.

59 D. S. Sigman, A. Mazumder and D. M. Perrin, *Chem. Rev.*, 1993, **93**, 2295–2316.

60 G. Tabbì, C. Cassino, G. Cavigiolio, D. Colangelo, A. Ghiglia, I. Viano and D. Osella, *J. Med. Chem.*, 2002, **45**, 5787–5795.

61 M. Roy, B. V. S. K. Chakravarty, C. Jayabaskaran, A. A. Karande and A. R. Chakravarty, *Dalton Trans.*, 2011, **40**, 4855–4864.

62 T. Storr, K. H. Thompson and C. Orvig, *Chem. Soc. Rev.*, 2006, **35**, 534–544.

63 K. H. Thompson and C. Orvig, *Dalton Trans.*, 2006, 761–764.

64 N. Fozia, A. Wüstholz, R. Kinscherf and N. Metzler-Nolte, *Angew. Chem., Int. Ed.*, 2005, **44**, 2429–2432.

65 S. S. Kelkar and T. M. Reineke, *Bioconjugate Chem.*, 2011, **22**, 1879–1903.

66 S. Santra, C. Kaittanis, O. J. Santiesteban and J. M. Perez, *J. Am. Chem. Soc.*, 2011, **133**, 16680–16688.

67 K. Stefflova, H. Li, J. Chen and G. Zheng, *Bioconjugate Chem.*, 2007, **18**, 379–388.

68 D. D. Perrin, W. L. F. Armarego and D. R. Perrin, *Purification of Laboratory Chemicals*, Pergamon Press, Oxford, 1980.

69 S. C. Sahoo and M. Ray, *Dalton Trans.*, 2007, 5148–5155.

70 S. C. Sahoo and M. Ray, *Dalton Trans.*, 2009, 3230–3236.

71 D. F. Evans, *J. Chem. Soc.*, 1959, 2003–2005.

72 D. F. Evans and T. A. James, *J. Chem. Soc., Dalton Trans.*, 1979, 723–726.

73 (*a*) J. D. McGhee and P. H. von Hippel, *J. Mol. Biol.*, 1974, **86**, 469–489; (*b*) M. T. Carter, M. Rodriguez and A. J. Bard, *J. Am. Chem. Soc.*, 1989, **111**, 8901–8911.

74 T. Mosmann, *J. Immunol. Methods*, 1983, **65**, 55–63.

75 J. E. Coligan, A. M. Kruisbeck, D. H. Margulies, E. M. Shevach and W. Strober, in *Related Isolation Procedures and Functional Assay, Current Protocols in Immunology*, ed. R. Coico, John Wiley & Sons, Inc., New York, 1995, p. 3.17.1.

76 J. L. McClintock and B. P. Ceresa, *Invest. Opthalmol. Vis. Sci.*, 2010, **51**, 3455–3461.